ACS Sustainable Chemistry & Engineering

pubs.acs.org/journal/ascecg

Research Article

Enhanced U(VI) Removal from Groundwater Using Amide-Functionalized Biopolymer-Based Adsorbent for a Practical Solution

Sonali Seth, Md Rabiul Islam, Tanmayaa Nayak, Amoghavarsha Ramachandra Kini, Sujan Manna, Bijesh K. Malla, Ankit Nagar, and Thalappil Pradeep*

Cite This: https://doi.org/10.1021/acssuschemeng.5c03058

Read Online

ACCESS | Metrics & More | Article Recommendations | Supporting Information

ABSTRACT: Uranium (U(VI)) contamination poses a serious threat to groundwater, which is the primary source of drinking water in many regions across the world. Removal of the predominant UO_2^{2+} species present in environmental water samples at affordable cost in resource-limited settings is challenging, particularly in the presence of competing ions. In this work, we introduced a sustainable approach for developing a biopolymer-based carboxymethyl cellulose (CMC)-chitosan (CH) adsorbent, free of metals, for selective removal of U(VI) from water. Amide functionalities, which serve as active sites for U(VI) capture, have been introduced by cross-linking CMC and CH with 4-aminobenzoic acid via 1-ethyl-3-(3-(dimethylamino)propyl)-carbodiimide (EDC) coupling. The adsorbent demonstrated excellent U(VI) removal efficiency in the presence of counterions such as transition metals, alkaline earth metals, and pentavalent vanadium (V(V)), which interfere strongly with many adsorbents. The composite showed 99.5% removal efficiency when tested on a field water sample containing 102 μg/L of U(VI). Mechanistic insights into U(VI) adsorption on the composite were obtained through infrared spectroscopy and X-ray photoelectron spectroscopy, which revealed that nitrogen in the amide functionalities facilitates interaction with U(VI). Raman measurements were performed to understand the speciation of U(VI) in solution at pH 7, which confirmed no change in the charge state of uranium in solution upon interaction with the composite. The adsorbed U(VI) can be easily removed by 10 mM HCl (10 mL) within 90 min of reaction, and the adsorbent can be reused. The adsorbent maintained a removal efficiency of more than 92% over three reactivation cycles. Cost of the composite was estimated to be around \$10 for treating 1 KL of contaminated water at a U(VI) concentration of 1000 μg/L. However, as *N*-hydroxysuccinimide and EDC reagents, used for the synthesis, are contributing more than >90% of the overall cost, further optimization or substitution of these reagents by industrial chemicals will ensure economic viability of the process.

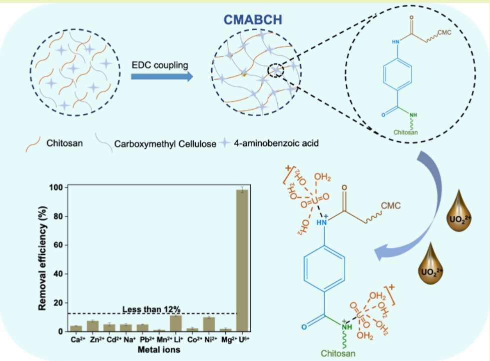

KEYWORDS: *Uranium, Adsorption, Biopolymers, Amide functionalities, Sustainability metrics*

INTRODUCTION

U(VI), a naturally occurring radionuclide, widely distributed in the earth's crust with an average concentration of around 2.7 mg/L, is found in various sources including rocks, minerals, groundwater, and seawater; in the latter it is at 3.3 μg/L.[1,2] Despite its crucial role in nuclear power generation and as a carbon-free energy source, it poses significant radiological and toxicological effects.[3] Although geogenic sources are the primary contributors of uranium in groundwater,[4] human activities such as mining, production and use of phosphate fertilizers, and nuclear power plant operations significantly contribute to its release into the environment.[4] Human exposure to uranium occurs through food, drinking water and dermal contact, causing adverse health effects, including nephrotoxicity and reproductive toxicity.[3,5] Uranium concentrations in the High Planes and Central Valley aquifers of the United States have been reported to reach 180 times the World Health Organization's (WHO) permissible limit of 30 μg/L.[6] In India, where 85% of rural drinking water supplies rely on groundwater, uranium contamination exceeds the WHO's limit in 18 states.[7−9] In groundwater systems, uranium predominantly exists in two oxidation states: U(IV) (as UO_2) and U(VI) (as UO_2^{2+}). U(IV) is sparingly soluble (~10^{-6} mol/kg), largely immobile, and typically precipitates under reducing conditions as insoluble minerals or complexes. In contrast, U(VI) is highly soluble, mobile, and environmentally toxic. A study by Patnaik et al. reported that elevated concentrations of U(VI) in the groundwater of Punjab are primarily attributed to the weathering of the Siwalik

Received: April 3, 2025
Revised: June 28, 2025
Accepted: July 1, 2025

mountains. Meanwhile, U(IV) tends to accumulate at the redox fronts within the paleo-channels of the Siwalik formations.[10] Furthermore, the presence of nitrates in groundwater can oxidize U(IV) to U(VI), enhancing its dissolution.[4] Depending on the availability of counterions, U(IV) can form stable, soluble complexes, thereby increasing its mobility and leaching potential in groundwater systems. U(IV) minerals readily convert to dissolved U(VI) species under oxidizing conditions.[6] U(VI) can also complex with other ions like carbonates, phosphates and humic substances (HS) present in water.[11,12] HS can interfere with and affect U(VI) adsorption. Liu et al. demonstrated that HS can mobilize U(VI) under reducing conditions.[13] Similarly, A. Krepelova et al. investigated the adsorption of U(VI) on kaolinite in the presence and absence of HS. Their study showed that pH plays a significant role in U(VI) sorption; at neutral pH, the formation of uranyl-humate complexes inhibits U(VI) adsorption onto kaolinite.[14] However, A. Kumar et al. have shown that carbonates exert a stronger influence on U(VI) sorption as compared to HS in the pH range 3.5−9.5.[15]

There are several methods for removing U(VI) from water, including membrane filtration,[16] electrocoagulation,[17] ion exchange,[18] and biological methods.[19] These methods are expensive and are effective only when the concentration of pollutants is high.[20] Among all the techniques, U(VI) removal via adsorption is the most cost-effective and efficient technique. Adsorption of contaminants onto a solid surface is a simple and well-known technology for heavy metal removal from water.[21] A variety of adsorbents, including zeolites,[22] biosorbents,[23] activated carbon,[24] carbon nanotubes,[25] clays,[26] metal oxides,[27] and metal−organic frameworks (MOFs),[28] have been reported for U(VI) removal from water.

In the following, we briefly review the literature on the use of biopolymer-based materials for U(VI) removal. Biopolymers like chitosan (CH) and cellulose, known for their biocompatibility, nontoxic character and multiple active sites, have been widely used for heavy metal remediation.[29] They have reactive functional groups in their matrix like hydroxyls (−OH), carboxylic acid (−COOH) and amine ($-NH_2$) that can be easily tuned to interact with heavy metals including U(VI).[30] CH, a naturally abundant biopolymer with $-NH_2$ groups, is a potential candidate for heavy metal removal from water.[31,32] However, it has poor chemical and mechanical stability in aqueous solutions,[33] rendering its usage. To overcome this limitation, it is crucial to develop novel adsorbents with improved stability and enhanced affinity for U(VI). Cross-linking of biopolymers is one such approach to enhance the stability of the adsorbents.[34] Moreover, cross-linking of biopolymers by introducing specific functionalities that serve as active sites enhances the heavy metal removal efficiency.[35] Carboxymethyl cellulose (CMC), an anionic derivative of cellulose having ether functionalities ($-O-CH_2COONa$), is particularly known for its ease of modification, and it provides active sites for cross-linking with other polymers.[36,37] Manzoor et al. demonstrated the cross-linking of CMC with CH using ethylenediaminetetraacetic acid (EDTA) for copper (Cu) removal from wastewater.[38] However, the preparation of the adsorbent requires *p*-toluene sulfonic acid (*p*-TSA), which is toxic,[39] and the reaction needs high temperatures. Similarly, Wang et al. modified CH using 3-indoleacetic acid in *p*-TSA for U(VI) removal from water, and the reaction needed elevated temperatures.[30] These methods are unsustainable due to reliance on high temperatures and organic solvents for adsorbent preparation. It is known that functional groups like phosphates,[12] imines,[40] amines,[41] carboxyls,[42] and amidoximes[43] form stable complexes with U(VI) and can be integrated into biopolymers to enhance their adsorption capacity as well as mechanical and chemical stability. It is also possible to introduce amide functionalities into biopolymers for enhanced U(VI) removal efficiency. Galindo et al. investigated the cosorption of uranyl and phosphates and the formation of uranyl phosphates on alumina surface at pH 3 through IR spectroscopy, highlighting the role of phosphates in enhancing uranyl adsorption on the surface of alumina.[44] Kushwaha et al. explored the adsorption of U(VI) on palm-shell-based adsorbent to understand the role of −COOH functionality in reducing U(VI) to U(V) and U(IV) through XPS, Extended X-ray Absorption Fine Structure (EXFAS) and IR spectroscopy.[45]

Several methods have been reported for the introduction of amide functionalities. For example, Wang et al. introduced amide groups to CH in the presence of *p*-TSA at 60 °C.[46] Additionally, Sabatini et al. have described approaches for amide bond formation focusing on sustainability and efficiency.[47] Various coupling agents, such as thionyl chloride, oxalyl chloride, and carbodiimide-based reagents like EDC and dicyclohexylcarbodiimide (DCC), are commonly used for amide bond synthesis. The choice of solvent and reaction temperature also significantly influences the efficiency and outcome of these reactions.

In this research, CMC and CH were chosen as precursors due to their abundance, nontoxicity, biocompatibility, active functional groups, low cost and ease of modification. A novel adsorbent (CMABCH) was developed by cross-linking CMC and CH with 4-aminobenzoic acid (PABA) to introduce amide functionalities through EDC coupling (details in materials and methods). EDC/NHS was selected due to its water solubility and compatibility with our reaction conditions, as many alternatives are water-insoluble. This method utilized the facile coupling of $-NH_2$ and −COOH to introduce amide functionalities in aqueous media.[48] Our work focused on elucidating the role of amide functionalities in enhancing U(VI) adsorption, with insights obtained through IR spectroscopy and Raman spectroscopy. Along with it, the mechanism of interaction of U(VI) with CMABCH was elucidated by XPS. Batch adsorption studies were conducted to examine the adsorption capacity of CMABCH, which demonstrated excellent adsorption capacity for U(VI) over a broad range of pH and in the presence of competing ions. Furthermore, CMABCH demonstrated excellent adsorption capacity over three reactivation cycles, highlighting its reusability and robustness. Real-field groundwater samples, containing U(VI) were collected from a well in Shamshabad village, Fazilka, Punjab State, India to evaluate the performance of the adsorbent, and we found a removal efficiency of 99.5% by CMABCH in the real-field sample.

■ EXPERIMENTAL SECTION

Materials. CMC and CH were purchased from Avantor Performance Materials India Ltd. and Pelican Biotech & Chemicals Laboratories Pvt. Ltd. (India), respectively. PABA was purchased from Merck Chemicals Pvt. Ltd. (India). EDC and NHS were purchased from Spectrochem Pvt. Ltd. (India). Uranyl nitrate ($UO_2(NO_3)_2.6H_2O$) was procured from Thomas Baker (Chemicals) Ltd. (India). Analytical-grade chemicals were utilized without additional purification. Porous filters were purchased from local

Scheme 1. (a) Schematic of the Synthesis of CMABCH through EDC Coupling Using Water as the Solvent.[a] (b) Schematic Illustration of the Use of CMABCH Filter for U(VI) Removal from Water. (c) HRSEM Image of Granular CMABCH Used for U(VI) Removal[b]

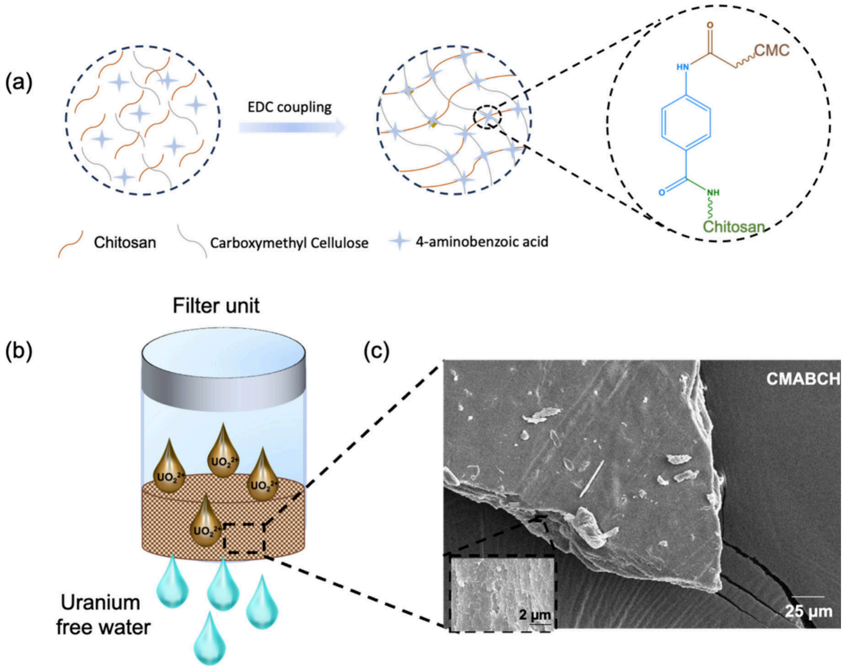

[a]The active sites of CMABCH convert U(VI) to U(IV), enhancing the adsorption capacity. [b]Inset shows an expanded HRSEM image of the selected region with a scale bar of 2 μm.

suppliers and deionized water (DI) was used throughout the experiments unless otherwise specified.

Synthesis of CMC−CH Adsorbent (CMABCH). A simple approach was employed to synthesize CMABCH. Initially, 2 g of CMC was dissolved in 100 mL of water and stirred for 30 min to achieve a uniform dispersion. Subsequently, 0.5 g each of EDC and NHS were added to the CMC solution, and the reaction mixture was stirred for 24 h. Following this, 2 g of PABA was introduced to the reaction mixture and stirred for an additional 12 h, facilitating the linkage of PABA to CMC via EDC coupling. To this reaction mixture, another 0.5 g of EDC and 0.5 g of NHS were added and the solution was stirred for another 24 h. Subsequently, 2 g of CH solution in 100 mL of 1% HCl was added to the mixture and incubated for 12 h. The resulting precipitate (CMABCH) was washed thoroughly with water and dried at 60 °C. Finally, the dried material was mechanically ground and sieved with a 200-μm sieve to obtain a granular powder. The composite was insoluble in water and the yield of the composite was about 4.2 g. The synthesis was performed under ambient conditions using water as the solvent, making the process greener and more sustainable. EDC and NHS were used as catalysts to facilitate amide bond formation. The dual functional groups of PABA ($-NH_2$ and $-COOH$) enabled it to function as a chelating ligand,[49] effectively cross-linking CMC and CH and facilitating amide bond formation as shown in Scheme 1a. The high-resolution scanning electron microscopy (HRSEM) image of CMABCH demonstrated granular and rough surface, making it suitable for its use in water purification cartridge as shown in Scheme 1b and 1c. Brunauer−Emmett−Teller (BET) surface area measurement was performed to analyze the structural framework of CMABCH, revealing a surface area of 20.6 m^2/g with an average pore size of 2.44 nm, making it a mesoporous material as shown in Figure S1.

Batch Adsorption Studies. U(VI) removal efficiency of the composite was checked by adding 30 mg of CMABCH to 10 mL of U(VI) spiked water at a concentration of 1000 μg/L. Water samples were collected at regular time intervals to determine the leftover U(VI) concentration. This was measured using Inductively Coupled Plasma Mass Spectrometry (ICP-MS) after acidifying the samples with 5% HNO_3. The maximum uptake capacity of U(VI) was calculated using eq 2 in Supporting Information.

pH Effect. pH-dependent studies were conducted to investigate the effect of pH on the adsorption of U(VI) on CMABCH. 30 mg of CMABCH was added to U(VI) spiked (1000 μg/L) DI water (10 mL), and pH was adjusted using 1 M NaOH/1 M HCl. After 2 h of reaction, the water samples were collected and analyzed by ICP-MS.

Interfering Ions. To evaluate the selectivity of CMABCH toward U(VI), an adsorption experiment was conducted with 10 mL water solution spiked with 1000 μg/L multimetal ions containing cadmium (Cd^{2+}), lead (Pb^{2+}), zinc (Zn^{2+}), manganese (Mn^{2+}), lithium (Li^{+}), nickel (Ni^{2+}), cobalt (Co^{2+}), sodium (Na^{+}), calcium (Ca^{2+}), magnesium (Mg^{2+}), and U^{6+}. Thirty mg CMABCH was added to the solution to check its selectivity for U(VI). Also, Since V(V) have properties similar to U(VI) and competes for active adsorption sites, batch adsorption study was carried out with 10 mL water spiked with almost equal concentrations (1000 μg/L) of U(VI) and V(V). Thirty mg of CMABCH was added to the solution to check the performance of CMABCH in the presence of V(V). Water sample was collected after 2 h, and ICP-MS analysis was performed. Further studies were performed to analyze the effect of common anions on U(VI) removal. A multianion mixture (10 mL) containing 1000 μg/L each of fluoride(F^-), chloride(Cl^-), bromide (Br^-), nitrate (NO_3^-), nitrite (NO_2^-), sulfates (SO_4^{2-}), and phosphates (PO_4^{3-}) was spiked with 1000 μg/L of U(VI) (10 mL) and ICP-MS analysis was done after 2h treatment with 30 mg of CMABCH.

Instrumentation. IR spectra were recorded using a PerkinElmer FT-IR spectrometer, keeping spectrometer resolution at 4 cm^{-1}. HRSEM images and Energy Dispersive X-ray Spectroscopy (EDS) mapping were carried out on a Thermo Scientific Verios G4 UC SEM. XPS measurements were performed with an Omicron Nanotechnology ESCA Probe TPD spectrometer, utilizing a Mg Kα X-ray source ($h\nu = 1253.6$ eV). A constant analyzer energy of 20 eV was applied for the measurements, and binding energies were calibrated with respect to the C 1s peak at 284.8 eV. Residual U(VI) concentration was analyzed using a PerkinElmer NexION 300X ICP-MS. Thermogravimetric analysis (TGA) was performed with a TA

https://doi.org/10.1021/acssuschemeng.5c03058
ACS Sustainable Chem. Eng. XXXX, XXX, XXX−XXX

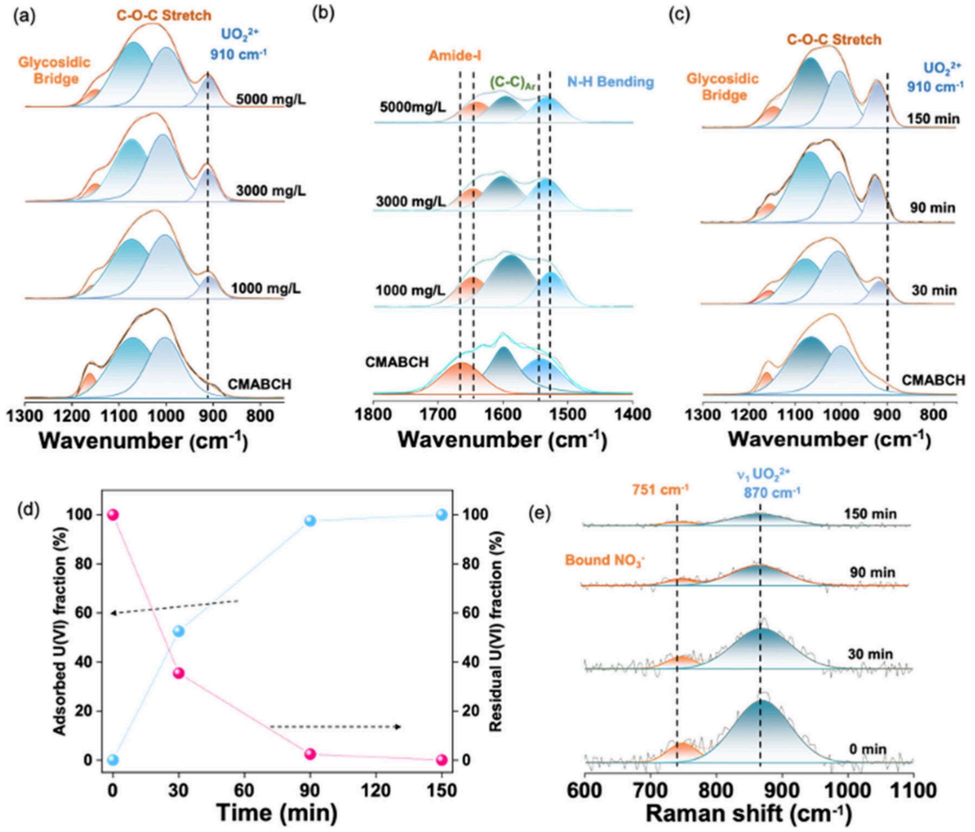

Figure 1. FTIR studies of CMABCH before and after U(VI) adsorption. Deconvoluted concentration-dependent IR spectra, before and after U(VI) adsorption (m-50 mg, V-10 mL, pH-7): (a) in the U(VI) antisymmetric region and (b) in the amide I and amide II regions. Deconvoluted time-dependent IR spectra ($U(VI)_o$-5000 mg/L, m-50 mg, V-10 mL, pH-7), (c) before and after U(VI) adsorption in the U(VI) antisymmetric region. (d) Adsorbed U(VI) fraction (%) in CMABCH and residual U(VI) fraction (%) in water, as a function of time. (e) Raman spectra of residual UO_2^{2+} species in solution after treatment with CMABCH at regular time intervals ($U(VI)_o$ - 5000 mg/L, m-50 mg, V-10 mL, pH-7).

Instruments Q500 Thermogravimetric Analyzer. The analysis was carried out under air and nitrogen atmospheres, covering a temperature range from room temperature to 900 °C, with a scan rate of 5 °C/min. Raman spectra were obtained using a CRM 200 micro Raman spectrometer of WiTec GmbH (Germany). The substrate was mounted on a sample stage of a confocal Raman spectrometer with 633 nm laser excitation. The treated water samples were taken on a glass substrate and analyzed keeping the laser and other parameters the same. BET surface area measurement was done using Micromeritics ASAP 2020 by degassing the sample at 120 °C for 12 h. Zeta potential studies were done using a Malvern Zetasizer Nano ZSP.

■ RESULTS AND DISCUSSION

Characterization of CMABCH, before and after U(VI) Adsorption. The IR spectra of CMABCH and its precursors, i.e., CMC, PABA, and CH were recorded to confirm the synthesis of CMABCH as shown in Figure S2. For CMABCH, a peak at 1598 cm^{-1}, corresponding to C−C aromatic stretching, confirmed the successful cross-linking of PABA to CMC and CH.[50,51] Additionally, shoulder peaks at 1660 cm^{-1} (amide-I) and 1540 cm^{-1} (amide-II) confirmed the amide bond formation.[52,53] A broad peak at 1000−1070 cm^{-1}, along with a shoulder peak at 1160 cm^{-1}, attributed to C−O−C stretching of glucopyranose ring,[54,55] further supported the cross-linking and formation of CMABCH. IR spectra depict the changes in the active sites of CMABCH on treatment with U(VI) solutions ranging from 1000 mg/L to 5000 mg/L, to determine the U(VI) adsorption mechanism at equilibrium. Figures 1a and 1b present the deconvoluted concentration-dependent IR of CMABCH, before and after U(VI) adsorption, in the regions corresponding to UO_2^{2+} antisymmetric stretch and amide band region, while the parent IR spectra of CMABCH, before and after U(VI) adsorption, are presented in Figure S3. The characteristic antisymmetric vibration of UO_2^{2+} at 940 cm^{-1} (as shown in Figure S4)[43] was red-shifted to 910 cm^{-1} upon U(VI) binding to CMABCH (as shown in Figure 1a), with increased intensity at higher U(VI) concentrations indicating high adsorption capacity of CMABCH. It is worth noting that the shift in the amide-I peak occurs from 1660 cm^{-1} to 1640 cm$^{-1,}$ and the amide-II peak shifts from 1540 cm^{-1} to 1530 cm^{-1}, along with reduction in −N-H band intensity with higher U(VI) concentrations suggests nitrogen interaction and complexation with U(VI), confirming the role of nitrogen of amide functionalities as active sites in U(VI) binding, shown in Figure 1b. The reaction mechanism is represented by eq 1.

$$\text{-C-CO-NH-} + [UO_2(H_2O)_5]^{2+} \rightarrow \text{C-(CO)-N}\cdots UO_2(H_2O)_4]^{+} + H^{+} \quad (1)$$

Further analysis included monitoring the IR spectra of CMABCH, before and after U(VI) adsorption at regular time intervals as shown in Figure S5. The deconvoluted time-dependent IR spectra in the region of UO_2^{2+} antisymmetric stretch are shown in Figure 1c, indicating that active sites on CMABCH reached saturation within 90 min, beyond which no

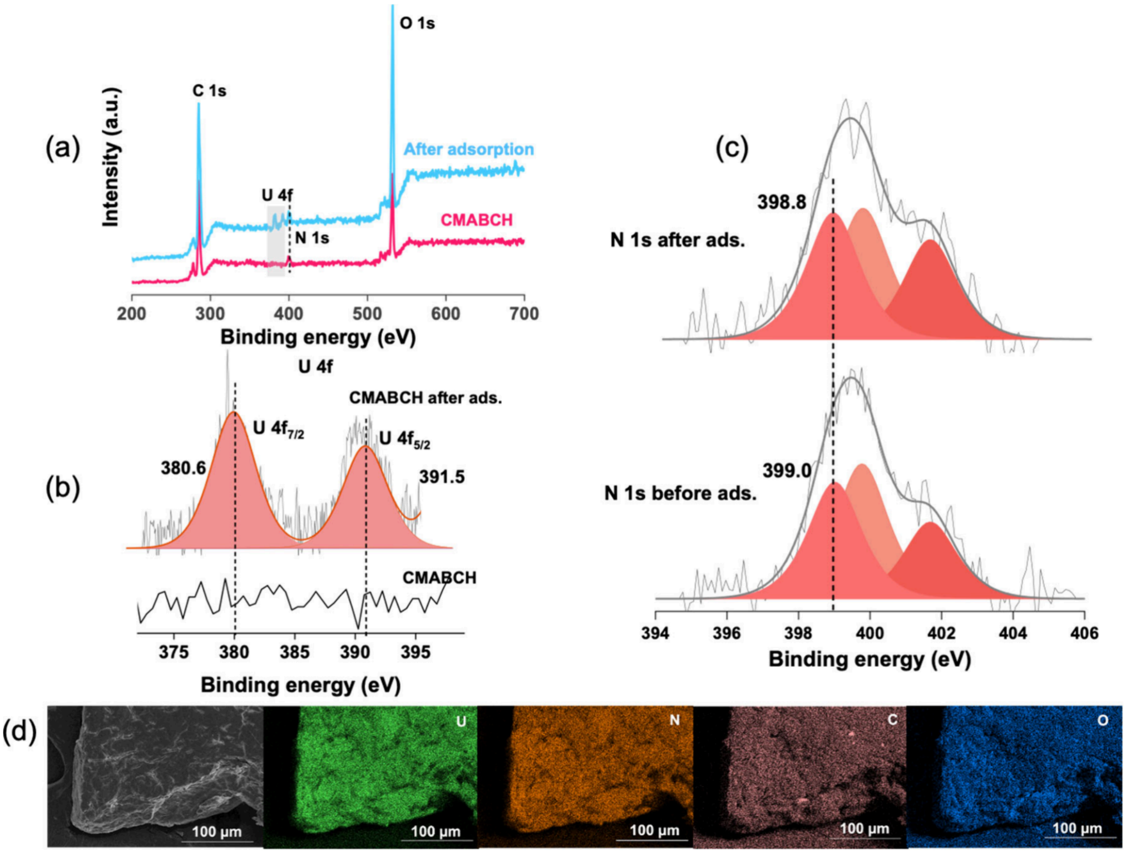

Figure 2. XPS survey spectra of (a) CMABCH before and after U(VI) adsorption.(b) U 4f regions of CMABCH, before and after U(VI) adsorption (U(VI)$_o$- 5000 mg/L, m-50 mg, V-10 mL, pH-7). (c) Deconvoluted XPS spectra of N 1s region before and after U(VI) adsorption. (d) HRSEM of CMABCH after U(VI) adsorption and corresponding EDS elemental mapping of U, N, C, and O (U(VI)$_o$ - 5000 mg/L, m-50 mg, V-10 mL, pH-7).

significant adsorption was observed. To quantify the availability of U(VI) adsorption in relation to the availability of active sites, the peak area at 914 cm^{-1} was used to estimate the fraction of U(VI) adsorbed with respect to the availability of active sites with time. The fraction (%) of U(VI) adsorbed was calculated using eq S1a (Supporting Information)[56] and compared with residual U(VI) fractions determined from ICP-MS data (Supporting Information, eq S1b). This strongly suggests that the active sites were fully occupied within 90 min, as all the amide functionalities were engaged in binding with U(VI). Additionally, Raman spectroscopic studies were performed at room temperature to understand the species of U(VI) in water over time at pH 7. The standard aqueous U(VI) solution (5000 mg/L, Figure 1e) showed two characteristic peaks at 870 cm^{-1} and 751 cm^{-1}, corresponding to UO_2^{2+} symmetric stretching and bound NO_3^- of $UO_2(NO_3)_2^0$, respectively.[57] Over time, the peak intensity of the U(VI) species in solution decreased, suggesting no change in U(VI) species in solution upon interaction with CMABCH, as shown in Figure 1e. Raman spectroscopy is particularly informative on the speciation of uranium in solution.

XPS provided further insights into U(VI) interaction with CMABCH. The survey spectra revealed C 1s, N 1s, and O 1s peaks, with additional peaks appearing after U(VI) adsorption due to U 4f, as shown in Figure 2a. Peaks for adsorbed U(VI) were detected at 380.6 eV (U 4f$_{7/2}$) and 391.5 eV (U 4f$_{5/2}$), with a 2 eV shift compared to standard UO_2^{2+}, suggesting a partial reduction of U(VI) to U(IV),[45] as presented in Figure 2b and Table 1. To further investigate the U(VI) adsorption process on CMABCH, deconvoluted XPS spectra before and after U(VI) adsorption were compared and the deconvoluted N 1s peaks were observed at 399.0 eV (R−N−H-C═O), 399.7 eV (N−C═O), and 401.3 eV ($-NH_3^+$), with a post adsorption major shift of C−N−H-C═O bond to 398.8 eV,

Table 1. Binding Energies (eV) of C 1s, O 1s, N 1s, and U 4f before and after U(VI) Adsorption onto CMABCH

Valence states	Samples	Binding energy (eV) before U(VI) adsorption	Binding energy (eV) after U(VI) adsorption	Reference
C 1s	C−C, C−N	284.7	284.7	53
	C−O, C−OH, C−N−C═O	286.3	286.4	53
	N−C═O	288.0	288.1	55
O 1s	C−O	530.4	530.5	30
	Aromatic C═O	531.7	531.8	58
N 1s	-C-NH−CO-	399.0	398.7	59
	N−C═O	399.7	399.6	60
	$-NH_3^+$	401.3	401.3	53
U 4f	U(VI) 4f$_{7/2}$	382.8		39
	U(VI) 4f$_{5/2}$	393.6		43
	U(IV) 4f$_{7/2}$		380.6	61
	U(IV) 4f$_{5/2}$		391.5	61

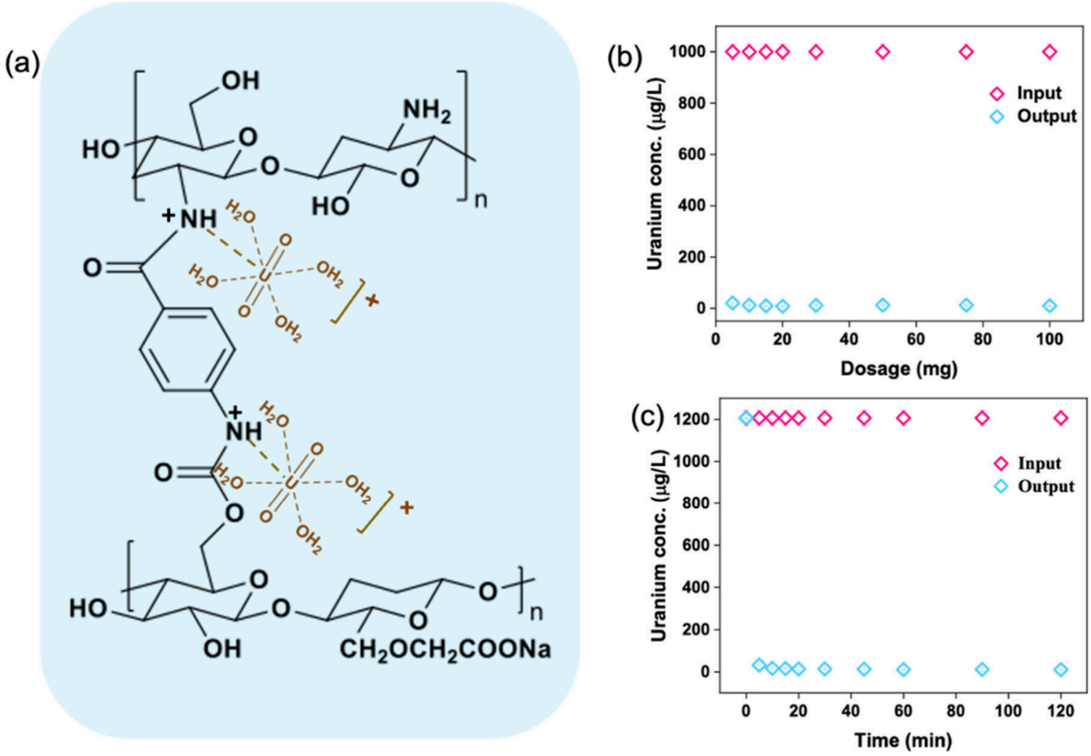

Figure 3. (a) Possible adsorption mechanism of U(VI) onto amide active sites of CMABCH. (b) Concentrations as a function of dosage of CMABCH.(Conditions- U(VI)$_o$-1000 μg/L, V-10 mL, pH-7). (c) U(VI) concentration as a function of contact time. (Conditions- U(VI)$_o$-1000 μg/L, m-30 mg,V-10 mL, pH-7).

indicating the interaction of nitrogen with U(VI) as shown in Figure 2c. The deconvoluted C 1s spectra (Figure S5) showed peaks for −C-C and −C-N bonds (284.7 eV), C−O, C−OH, and C−N−C═O bonds (286.3 eV), and N−C═O bonds (288.0 eV) with no significant change after U(VI) adsorption. Similarly, no notable shift in binding energies of O 1s was observed, as shown in Figure S6 and Table 1. These findings suggest that the nitrogen atoms in amide groups serve as the active sites for U(VI) immobilization on CMABCH, facilitating charge transfer and contributing to the reduction of U(VI) to U(IV),[55] consistent with the IR studies. Based on the observations from IR and XPS, the proposed mechanism involves the amide functionalities providing active sites for U(VI) binding and chelation. Upon adsorption of U(VI) onto the surface of CMABCH, the lone pair electrons on the nitrogen atoms facilitate charge transfer to U(VI), leading to its partial reduction to U(IV). This charge transfer alters the electronic environment surrounding U(VI), as evidenced by the shift in N 1s binding energy from 399.0 to 398.8 eV and U 4f shift to 380.6 and 391.5 eV, confirming U(VI) binding and reductive adsorption on the CMABCH surface, indicating that the reduction step plays an essential role in the adsorption process.

The surface morphology of CMABCH was examined before and after U(VI) adsorption using HRSEM. The HRSEM image of granular CMABCH, along with its corresponding elemental mapping, is provided in Figure S7. The high carbon and oxygen content were coming from the polymer backbone, and the nitrogen was coming from amide functionalities. No changes in the morphology of CMABCH were observed after exposure to a concentrated U(VI) solution and U(VI) was homogeneously adsorbed on the surface of CMABCH and the corresponding elemental mapping is shown in Figure 2d. This confirms the successful adsorption of U(VI) onto CMABCH. Figure S8 shows powder XRD patterns of the precursors CMC,[62] PABA,[63] CH,[64] CMABCH, and CMABCH after U(VI) adsorption. In the case of CMABCH, the diffraction patterns display a peak at 15.5° along with a broad hump between 16° and 30°, originating from its precursors, which confirms the amorphous−crystalline nature of CMABCH. Following U(VI) adsorption, only a broad peak is observed, indicating the amorphous nature of CMABCH and the disappearance of distinct crystallinity peaks as a result of the adsorption process.

The studies have shown the interactions of nitrogen, phosphonate and oxygen functional groups with U(VI).[9,65] Based on our studies, we can interpret the probable binding of U(VI) with the nitrogen of amide functionalities, dependent on the availability of amide sites, supported by IR and XPS studies, as shown in Figure 3a.

Control studies were conducted with CMC which removed 100−200 μg/L of U(VI) from 1000 μg/L U(VI) spiked water, suggesting that it could be used as a platform for U(VI) adsorption. Thermal stability of CMABCH was analyzed by TGA. Analysis was performed under nitrogen and air atmosphere within the temperature range from room temperature to 900 °C at the heating rate of 5 °C min^{-1} as shown in Figure S9. It is known that CMC and CH start decomposing at 250 and 175 °C, respectively,[30,38] while PABA degrades within the temperature range of 200−300 °C.[66] In the case of CMABCH, a three-step degradation was observed. Around 8% weight loss was due to the adsorbed water molecules below 120 °C. CMABCH exhibited thermal stability until 235 °C. A significant mass loss of 45% occurred in the temperature range of 238 to 400 °C, due to the decomposition of organic molecules into low molecular weight organic compounds.[67]

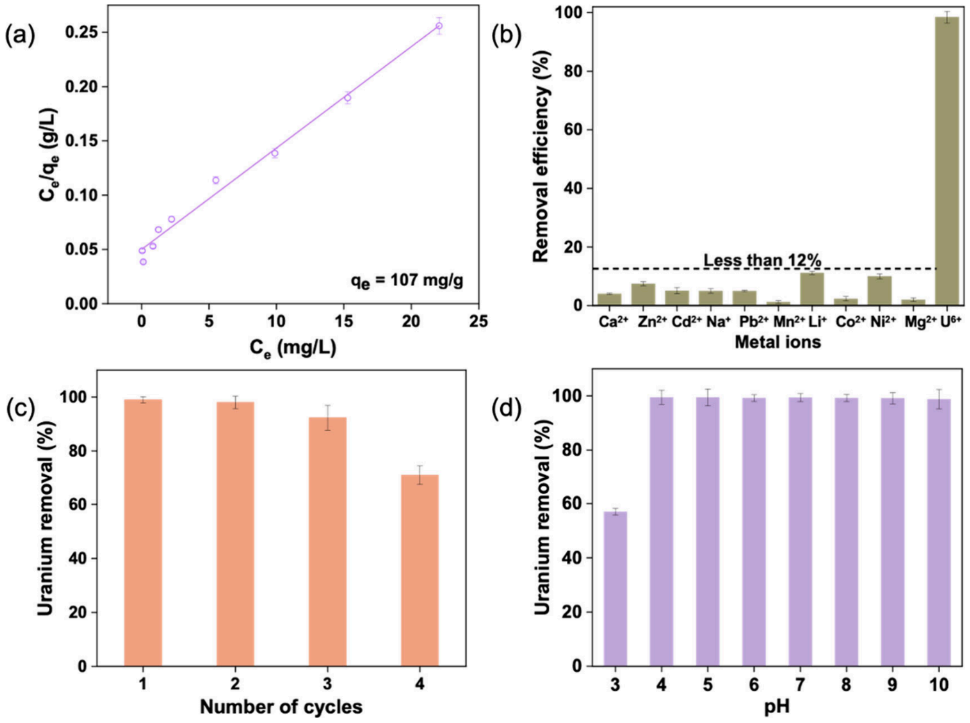

Figure 4. (a) Langmuir adsorption isotherm of CMABCH (m-5 mg, V-10 mL, pH-7). (b) Selective U(VI) capture from 10-ions mixture solution (M_o and $U(VI)_o$-1000 μg/L, m-30 mg, V-10 mL, pH-7). (c) Batch adsorption studies for adsorption−desorption cycles of U(VI) on CMABCH ($U(VI)_o$-1000 μg/L, m-30 mg, V-10 mL, pH-7). (d) Batch adsorption studies of CMABCH as a function of pH ($U(VI)_o$-1000 μg/L, m-30 mg, V-10 mL).

The final degradation of CMABCH, from 400 to 600 °C, was attributed to the complete degradation of CMABCH to CO_2 and H_2O.[68] We infer that the cross-linking of CH and CMC enhanced the thermal stability of the composite as compared to their pristine forms.

Batch Studies of U(VI) Adsorption on CMABCH. Figure 3 illustrates the performance of CMABCH for U(VI) adsorption, derived from batch studies. Ten mL of 1000 μg/L U(VI) spiked water was treated with CMABCH and its performance was evaluated. Different dosages of CMABCH ranging from 2 mg to 100 mg were checked and we found that less than 30 mg of CMABCH was enough to reduce the concentration of U(VI) below 10 μg/L within 2 h, as shown in Figure 3b. CMABCH also exhibited faster uptake kinetics as shown in Figure 3c. CMABCH showed high capacity to rapidly reduce the concentration of U(VI) below 10 μg/L, dependent on the number of active sites available for U(VI) adsorption. To analyze the kinetics data of U(VI) adsorption onto CMABCH, Ho's pseudo-second-order model was applied. The linear form of the equation used is presented in eq S3 (Supporting Information). The plot of t/q_e versus time gave a linear fit for U(VI) adsorption, as shown in Figure S10, with a correlation coefficient of 1 indicating that chemical adsorption[69] is the primary mechanism for U(VI) removal. Furthermore, it also suggests that the rate determination step is influenced by the availability of active adsorption sites[20] and the involvement of amide functionalities in U(VI) adsorption, as supported by the IR and XPS analysis discussed in Figures 1 and 2.

The maximum U(VI) uptake capacity of CMABCH was evaluated by introducing it into U(VI) spiked water, with U(VI) concentrations ranging from 1 to 100 mg/L at neutral pH. The Langmuir isotherm model was used to understand the influence of equilibrium concentration on the adsorption capacity of CMABCH. This model assumes that adsorption occurs at discrete, homogeneous sites on the adsorbent surface, forming a monolayer at equilibrium with no lateral interaction between adsorbed molecules. A plot of C_e/q_e versus C_e resulted in a linear fit using the eq S4 (Supporting Information), consistent with the Langmuir model. The adsorption isotherm gave the maximum adsorption capacity (q_{max}) of 107 mg/g for CMABCH, with a strong correlation coefficient of 0.99 as shown in Figure 4a. This confirms monolayer adsorption, which is also in agreement with Freundlich isotherm (Figure S11) having less R^2 value and n value greater than unity, confirming chemical adsorption (Table 2).[70]

Table 2. Parameters of the Adsorption Isotherm Models for U(VI) Adsorption

Langmuir model		Freundlich model		
q_{max} (mg/g)	R^2	K_F ($mg^{1-n}\cdot L^n/g$)	n	R^2
107	0.99	10.54	2.07	0.95

The performance of CMABCH was assessed for its selectivity toward U(VI) in the presence of competing metal ions at neutral pH. A selectivity study was conducted using a mixed solution containing 1000 μg/L (10 mL) Cd^{2+}, Pb^{2+}, Zn^{2+}, Mn^{2+}, Li^+, Ni^{2+}, Co^{2+}, Na^+, Ca^{2+}, Mg^{2+}, and U^{6+} as shown in Figure 4b. Figure 4b presents the removal efficiencies of individual ions by CMABCH within the mixture. CMABCH exhibited complete removal of U^{6+}, while the removal efficiencies for the other metal ions were below 12%, demonstrating exceptional selectivity for U(VI) over the coexisting ions in the same mixture. Since V(V) is the major

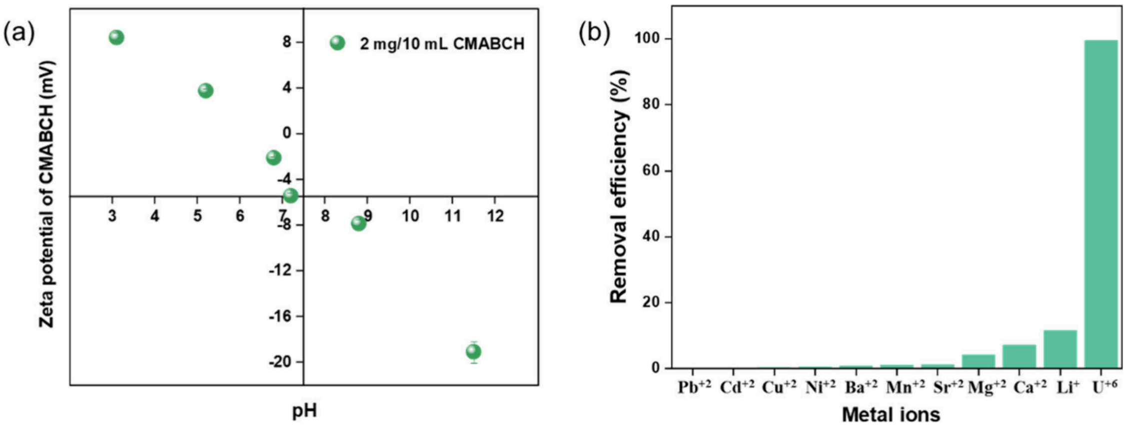

Figure 5. (a) Zeta potential vs pH (pH window 3−11) for CMABCH in water (2 mg in 10 mL). (b) U(VI) removal efficiency of CMABCH of groundwater containing 102 μg/L U(VI) and other coexisting ions. (m-30 mg, V-10 mL).

Table 3. Comparison of Adsorption Capacities of Other Cellulose/CH-Based Reported Materials for U(VI)

S.no.	Adsorbents	Uptake capacity (mg/g)	Optimum pH	Time (min)	Reusability	Reference
1	Deacetylated chitosan	17.44	3.5	1440	3	75
2	Chitosan modified phosphate rock	8.06	2.5	300	-	76
3	Chitosan bentonite composite	49.09	8	60	6	77
4	Hyper cross-linked polymer	46.74	8	70	4	78
5	Functionalized natural cellulose fibres	16.0	-	240	-	79
6	CMABCH	107	neutral	120	3	This work

competitor during U(VI) extraction from seawater, CMABCH performance was evaluated for U(VI) in the presence of V(V) and it was observed that CMABCH removed 99% U(VI) and only 30% V(V), as shown in Figure S12. This selectivity is attributed to the preferential interaction of V(V) with imide-dioxime groups.[71,72] Superior selectivity for U(VI) over other ions is due to the strong interaction of U(VI) with nitrogen atoms in the amide functionalities within CMABCH. These studies align well with IR and XPS analysis, further confirming the affinity of CMABCH for U(VI). Additionally, to assess the adsorption capacity of CMABCH in the presence of common anions, a multianion water mixture containing 1000 μg/L each of F^-, Cl^-, Br^-, NO_3^-, NO_2^-, SO_4^{2-}, and PO_4^{3-} was spiked with 1000 μg/L of U(VI) (10 mL). Under these conditions, CMABCH also achieved a U(VI) removal efficiency of 98%. The reusability of CMABCH was evaluated across multiple cycles as shown in Figure 4c. The adsorbent was recovered by centrifugation to minimize material loss, and the adsorbed U(VI) was effectively desorbed using 10 mM HCl (10 mL) within 90 min, and the composite retained a removal efficiency of 70% after three consecutive cycles. Comparative testing of various eluents (Table S1) showed low desorption efficiencies, while higher concentrations of HCl damaged the CMABCH structure and reduced its adsorption performance. In contrast, mild 10 mM HCl (10 mL) treatment efficiently desorbed UO_2^{2+} without compromising the functional groups of CMABCH, as confirmed by post-treatment IR analysis (Figure S13). Notably, the amide functionalities were retained for consecutive adsorption−desorption first cycle. However, after the third cycle, the composite exhibited a reduction in U(VI) removal efficiency to 70%, accompanied by damage to the amide functionalities, as evidenced in Figure S13. This deterioration is likely due to cumulative HCl exposure, which appears to degrade amide groups beyond the third cycle. Additionally, the appearance of a peak at 910 cm^{-1} in the IR spectrum suggests the presence of residual adsorbed U(VI), contributing to the decreased efficiency observed after three cycles. Note that U(VI) removal efficiency was evaluated over a wide pH range (pH 3−10), as illustrated in Figure 4d. The composite demonstrated excellent U(VI) removal efficiency between pH 4 and 10, with reduced efficiency at pH 3. The decline at lower pH is likely due to the protonation of amide functionalities[73] and competitive adsorption of H^+ ions, which interferes with UO_2^{2+} adsorption, reducing U(VI) removal efficiency. These observations align with the reusability of CMABCH, as the adsorbed U(VI) could be desorbed using 10 mM HCl. Changes in the pH not only affect the surface charge of the adsorbent but also influence the U(VI) speciation.[33]

Zeta potential studies were conducted to examine the surface charge of CMABCH to understand the preference of U(VI) adsorption. The zeta potential shifted from +8 mV at pH 3 to −20 mV at pH 12, as shown in Figure 5a. As the pH changed from acidic to neutral media, zeta potential shifted from positive to negative indicating reduced protonation of amide functionalities. At neutral pH, CMABCH acquired negative surface charge, enhancing the electrostatic attraction between the adsorbent and the UO_2^{2+}, thereby improving the removal efficiency. However, at very high pH beyond 10, CMABCH became highly negatively charged, leading to repulsions between CMABCH and the uranium species and decreasing the U(VI) removal efficiency.[74] To gain insights into U(VI) removal efficiency of CMABCH in real field samples, groundwater samples were collected from a well in Shamshabad village, Fazilka, Punjab. The water samples had a high concentration of U(VI), i.e. 102 μg/L, with other chemical characteristics as shown in Table S2. The field water exhibited high alkalinity, approximately 240 mg/L, elevated concentrations of SO_4^{2-} and Cl^-, while the PO_4^{3-} concentration was negligible, remaining below the detection limit. The adsorbent demonstrated a remarkable removal capacity, achieving 99.5% U(VI) removal. It effectively reduced U(VI) concentration to levels within the permissible limit set by WHO, even in the presence of coexisting ions as shown in Figure 5b.

The U(VI) adsorption capacity of CMABCH was compared with the existing composites and CMABCH showed higher U(VI) removal efficiency as shown in Table 3.

Aspects of Sustainability. The extent of "greenness" of this technology was assessed through mass-based sustainability parameters, with the formulas mentioned in the Supporting Information (eqs S7−S10).

Raw Materials. CMC and CH were used majorly because of their nontoxicity, renewable and biodegradable nature, with water being used as the solvent. The mass intensity (excluding water) came out to be 1.9, while water intensity was 47.6. The mass intensity could be further reduced to 1 by minimizing composite loss during filtration and washing. The reaction mass efficiency was determined to be 52.5%.

Resulting Emissions. The synthesis of the composite avoided the use of toxic harmful solvents. The E factor (environmental factor) was calculated to be 0.8 (without solvent recovery), indicating minimum emissions. NHS and EDC were removed through washing. The spent adsorbent may be processed similar to other such adsorbents following an evaluation of toxicity characteristic leaching procedure (TCLP), causing negligible environmental impact.[31] U(VI) was desorbed using 10 mM HCl (10 mL), and the acidic effluent generated during this process can be subsequently neutralized with NaOH and $CaCO_3$. Specifically, 0.4 g of NaOH and 0.5 g of $CaCO_3$ are sufficient to treat 1000 mL of 10 mM HCl solution.[80]

Economic Analysis. A cost analysis of the composite revealed that the composite can give uranium-free water at an approximate cost of $10/1000L. This cost, based on the cost of laboratory reagents, equipment use and labor, can be reduced by optimizing or substituting NHS/EDC with industrial raw materials, improving economic viability of the technology. According to the commercially available raw materials, the cost of CMC, CH and PABA (per kg) is around $10 whereas the cost of EDC/NHS (per kg) is approximately $50 which contributes to the total cost in the synthesis of CMABCH. Various alternative coupling agents are available for amide bond synthesis. For instance, Elschner et al. reported the synthesis of cellulose carbamate using phenyl chloroformate.[81] However, this reaction was carried out in organic solvents, under inert conditions, and at elevated temperatures. Such processes tend to be highly energy-intensive and generate significant amounts of secondary waste. Similarly, Wang et al. modified and introduced amide functionalities with the help of chloroformate at high temperatures.[82] While less expensive reagents such as oxalyl chloride or chloroformates could be considered for industrial-scale applications, their successful implementation would require substantial optimization of reaction conditions, including solvent systems and temperature controls, to achieve efficient and sustainable processes. A thorough techno-economic and process optimization study would be essential before considering the alternatives for industrial-scale optimization. However, a cost reduction by an order of magnitude is expected considering the cost of alternate reagents.

CONCLUSIONS

In this work, we present an eco-friendly method to cross-link CMC and CH by incorporating amide functionalities for efficient U(VI) removal from water. The removal mechanism involves the initial coordination of U(VI) ions with the nitrogen atoms of amide functionalities, followed by charge transfer and subsequent reduction to U(IV) as confirmed by IR and XPS. HRSEM analysis confirmed that the surface morphology remained the same after saturation with uranium. The adsorption capacity of CMABCH reached 107 mg/g, determined from the Langmuir adsorption model, which is superior as compared to other reported cellulose/chitosan materials. The adsorbent exhibited excellent U(VI) removal efficiency in the presence of other counterions, and the composite could be easily recovered and reused, giving a high U(VI) removal efficiency of more than 92% over three reactivation cycles. Its efficiency in removing U(VI) from groundwater in Punjab state, India, in the presence of many competing ions, highlights its potential as an excellent composite for drinking water decontamination.

ASSOCIATED CONTENT

Supporting Information

The Supporting Information is available free of charge at https://pubs.acs.org/doi/10.1021/acssuschemeng.5c03058.

> Equations used in the main text; BET surface area plots (a) N_2 adsorption−desorption plot. (b) Pore size distribution; IR spectra of CMABCH and its precursors i.e., CMC, 4-PABA, and CH; IR spectra of CMABCH, before and after treatment with various concentrations of U(VI); IR spectra of standard $(UO_2(NO_3)_2.6H_2O)$; IR spectra of CMABCH, before and after U(VI) adsorption, at regular time intervals; Deconvoluted XPS spectra of (a) C 1s and (b) O 1s regions before and after U(VI) adsorption (bottom to top); HRSEM image of CMABCH and its corresponding elemental mapping; Powder XRD of CMABCH, its precursors i.e. CMC, PABA and CH and CMABCH after U(VI) adsorption; TGA of CMABCH in air and nitrogen atmospheres from room temperature to 900 °C at a scan rate of 5 °C min^{-1}; Ho's pseudo-second-order kinetic plot for the adsorption of U(VI) onto CMABCH; Freundlich isotherm plot for the adsorption of U(VI) on CMABCH; Removal efficiency of CMABCH when U(VI) and V(V) coexist; Desorption efficiencies by various eluents; FTIR of CMABCH after adsorption−desorption cycles; Chemical parameters for the groundwater sample from the well in Shamshabad village, Fazilka, Punjab, India (PDF)

AUTHOR INFORMATION

Corresponding Author

Thalappil Pradeep − *DST Unit of Nanoscience (DST UNS) and Thematic Unit of Excellence (TUE), Department of Chemistry, Indian Institute of Technology Madras, Chennai 600036, India; International Centre for Clean Water, IIT Madras Research Park, Chennai 600113, India;* orcid.org/0000-0003-3174-534X; Email: pradeep@iitm.ac.in

Authors

Sonali Seth – *DST Unit of Nanoscience (DST UNS) and Thematic Unit of Excellence (TUE), Department of Chemistry, Indian Institute of Technology Madras, Chennai 600036, India*

Md Rabiul Islam – *DST Unit of Nanoscience (DST UNS) and Thematic Unit of Excellence (TUE), Department of Chemistry, Indian Institute of Technology Madras, Chennai 600036, India;* orcid.org/0000-0001-6454-4013

Tanmayaa Nayak – *DST Unit of Nanoscience (DST UNS) and Thematic Unit of Excellence (TUE), Department of Chemistry, Indian Institute of Technology Madras, Chennai 600036, India*

Amoghavarsha Ramachandra Kini – *DST Unit of Nanoscience (DST UNS) and Thematic Unit of Excellence (TUE), Department of Chemistry, Indian Institute of Technology Madras, Chennai 600036, India;* orcid.org/0009-0003-6863-7729

Sujan Manna – *DST Unit of Nanoscience (DST UNS) and Thematic Unit of Excellence (TUE), Department of Chemistry, Indian Institute of Technology Madras, Chennai 600036, India*

Bijesh K. Malla – *DST Unit of Nanoscience (DST UNS) and Thematic Unit of Excellence (TUE), Department of Chemistry, Indian Institute of Technology Madras, Chennai 600036, India*

Ankit Nagar – *DST Unit of Nanoscience (DST UNS) and Thematic Unit of Excellence (TUE), Department of Chemistry, Indian Institute of Technology Madras, Chennai 600036, India*

Complete contact information is available at:
https://pubs.acs.org/10.1021/acssuschemeng.5c03058

Notes

The authors declare no competing financial interest.

■ ACKNOWLEDGMENTS

The authors thank the Sophisticated Analytical Instrumental Facility (SAIF) IIT Madras for TGA measurements and the Department of Chemistry, IIT Madras. T.P. acknowledges financial support from the Ministry of Mines (MOM), India (SP21221094CYMOMI002505), funding from SERB SUPRA (Grant SPR/2021/000439), and the Centre of Excellence on Molecular Materials and Functions under the Institution of Eminence scheme of IIT Madras. S.S. thanks the Ministry of Human Resource Development, Prime Minister's Research Fellowship, Government of India. The authors also thank the Department of Science and Technology, Government of India, for supporting our research program on nanomaterials.

■ REFERENCES

(1) Smedley, P. L.; Kinniburgh, D. G. Uranium in Natural Waters and the Environment: Distribution, Speciation and Impact. *Appl. Geochem.* **2023**, *148*, No. 105534.

(2) Daniel, R.; Tripathi, D.; Singh, S.; Sharma, N.; Yuvraaj, A.; Katyal, D.; Kumar, V. Uranium: Occurrence, Distribution across India and Its Potential Health Effects. *J. Radioanal. Nucl. Chem.* **2022**, *331* (7), 2805–2815.

(3) Ma, M.; Wang, R.; Xu, L.; Xu, M.; Liu, S. Emerging Health Risks and Underlying Toxicological Mechanisms of Uranium Contamination: Lessons from the Past Two Decades. *Environ. Int.* **2020**, *145*, No. 106107.

(4) Balaram, V.; Rani, A.; Rathore, D. P. S. Uranium in Groundwater in Parts of India and World: A Comprehensive Review of Sources, Impact to the Environment and Human Health, Analytical Techniques, and Mitigation Technologies. *Geosystems Geoenvironment* **2022**, *1* (2), No. 100043.

(5) Zhang, L.; Chu, J.; Xia, B.; Xiong, Z.; Zhang, S.; Tang, W. Health Effects of Particulate Uranium Exposure. *Toxics* **2022**, *10* (10), 575.

(6) Nolan, J.; Weber, K. A. Natural Uranium Contamination in Major U.S. Aquifers Linked to Nitrate. *Environ. Sci. Technol. Lett.* **2015**, *2* (8), 215–220.

(7) Verma, M.; Loganathan, V. A. Hydrogeochemical Constraints on Uranium Contamination of Groundwater for Drinking Water Supplies and Associated Health Risks. *Groundw. Sustain. Dev.* **2023**, *23*, No. 100973.

(8) Bala, R.; Karanveer; Das, D. Occurrence and Behaviour of Uranium in the Groundwater and Potential Health Risk Associated in Semi-Arid Region of Punjab, India. *Groundw. Sustain. Dev.* **2022**, *17*, No. 100731.

(9) Nayak, T.; Mukherjee, S.; Kini, A. R.; Islam, M. R.; Nagar, A.; Seth, S.; Pradeep, T. Cellulose-Derived Nanomaterials for Affordable and Rapid Remediation of Uranium in Water. *ACS Sustain. Chem. Eng.* **2025**, *13* (4), 1838–1850.

(10) Patnaik, R.; Lahiri, S.; Chahar, V.; Naskar, N.; Sharma, P. K.; Avhad, D. K.; Bassan, M. K. T.; Knolle, F.; Schnug, E.; Srivastava, A. Study of Uranium Mobilization from Himalayan Siwaliks to the Malwa Region of Punjab State in India. *J. Radioanal. Nucl. Chem.* **2016**, *308* (3), 913–918.

(11) Kopylova, Y.; Guseva, N.; Shestakova, A.; Khvaschevskaya, A.; Arakchaa, K. Uranium and Thorium Behavior in Groundwater of the Natural Spa Area "Choygan Mineral Water" (East Tuva). *IOP Conf. Ser. Earth Environ. Sci.* **2015**, *27*, No. 012034.

(12) Lehtonen, J.; Hassinen, J.; Kumar, A. A.; Johansson, L.-S.; Mäenpää, R.; Pahimanolis, N.; Pradeep, T.; Ikkala, O.; Rojas, O. J. Phosphorylated Cellulose Nanofibers Exhibit Exceptional Capacity for Uranium Capture. *Cellulose* **2020**, *27* (18), 10719–10732.

(13) Luo, W.; Gu, B. Dissolution and Mobilization of Uranium in a Reduced Sediment by Natural Humic Substances under Anaerobic Conditions. *Environ. Sci. Technol.* **2009**, *43* (1), 152–156.

(14) Křepelová, A.; Sachs, S.; Bernhard, G. Uranium(VI) Sorption onto Kaolinite in the Presence and Absence of Humic Acid. *Radiochim. Acta* **2006**, *94* (12), 825–833.

(15) Kumar, A.; Rout, S.; Mishra, M. K.; Karpe, R.; Ravi, P. M.; Tripathi, R. M. Impact of Particle Size, Temperature and Humic Acid on Sorption of Uranium in Agricultural Soils of Punjab. *SpringerPlus* **2015**, *4* (1), 262.

(16) Shen, J.; Schäfer, A. Removal of Fluoride and Uranium by Nanofiltration and Reverse Osmosis: A Review. *Chemosphere* **2014**, *117*, 679–691.

(17) Choi, A. E. S.; Futalan, C. C. M.; Yee, J.-J. Fuzzy Optimization for the Removal of Uranium from Mine Water Using Batch Electrocoagulation: A Case Study. *Nucl. Eng. Technol.* **2020**, *52* (7), 1471–1480.

(18) Zhou, S.; Dong, F.; Qin, Y. High Efficiency Uranium(VI) Removal from Wastewater by Strong Alkaline Ion Exchange Fiber: Effect and Characteristic. *Polymers* **2023**, *15* (2), 279.

(19) Chowdhury, A. A.; Basak, N.; Islam, E. Removal of Uranium from Water Using Biofilm of Uranium Sensitive Methylobacterium Sp. *J. Hazard. Mater. Adv.* **2023**, *10*, No. 100296.

(20) Mukherjee, S.; Kumar, A. A.; Sudhakar, C.; Kumar, R.; Ahuja, T.; Mondal, B.; Srikrishnarka, P.; Philip, L.; Pradeep, T. Sustainable and Affordable Composites Built Using Microstructures Performing Better than Nanostructures for Arsenic Removal. *ACS Sustain. Chem. Eng.* **2019**, *7* (3), 3222–3233.

(21) Qasem, N. A. A.; Mohammed, R. H.; Lawal, D. U. Removal of Heavy Metal Ions from Wastewater: A Comprehensive and Critical Review. *Npj Clean Water* **2021**, *4* (1), 36.

(22) Camacho, L. M.; Deng, S.; Parra, R. R. Uranium Removal from Groundwater by Natural Clinoptilolite Zeolite: Effects of pH and

Initial Feed Concentration. *J. Hazard. Mater.* **2010**, *175* (1−3), 393−398.

(23) Embaby, M. A.; Haggag, E. A.; El-Sheikh, A. S.; Marrez, D. A. Biosorption of Uranium from Aqueous Solution by Green Microalga Chlorella Sorokiniana. *Environ. Sci. Pollut. Res.* **2022**, *29* (38), 58388−58404.

(24) Aslani, C. K.; Amik, O. Active Carbon/PAN Composite Adsorbent for Uranium Removal: Modeling Adsorption Isotherm Data, Thermodynamic and Kinetic Studies. *Appl. Radiat. Isot.* **2021**, *168*, No. 109474.

(25) Zhuang, S.; Wang, J. Poly Amidoxime Functionalized Carbon Nanotube as an Efficient Adsorbent for Removal of Uranium from Aqueous Solution. *J. Mol. Liq.* **2020**, *319*, No. 114288.

(26) Zahran, F.; El-Maghrabi, H. H.; Hussein, G.; Abdelmaged, S. M. Fabrication of Bentonite Based Nanocomposite as a Novel Low Cost Adsorbent for Uranium Ion Removal. *Environ. Nanotechnol. Monit. Manag.* **2019**, *11*, No. 100205.

(27) Yu, Z.; Li, Q.; Liao, J.; Zhang, Y.; Zhang, L.; Zhu, W. Efficient Removal of Uranium (VI) by Nano-Manganese Oxide Materials: A Synthetic Experimental and Mechanism Studies. *J. Alloys Compd.* **2021**, *868*, No. 159069.

(28) Song, Y.; Li, H.; Shan, T.; Yang, P.; Li, S.; Liu, Z.; Liu, C.; Shen, C. MOF-Implanted Poly (Acrylamide-Co-Acrylic Acid)/Chitosan Organic Hydrogel for Uranium Extraction from Seawater. *Carbohydr. Polym.* **2023**, *302*, No. 120377.

(29) Nasrollahzadeh, M.; Sajjadi, M.; Iravani, S.; Varma, R. S. Starch, Cellulose, Pectin, Gum, Alginate, Chitin and Chitosan Derived (Nano)Materials for Sustainable Water Treatment: A Review. *Carbohydr. Polym.* **2021**, *251*, No. 116986.

(30) Wang, Y.; Ai, Y.; Liu, X.; Chen, B.; Zhang, Y. Indole-Functionalized Cross-Linked Chitosan for Effective Uptake of Uranium(vi) from Aqueous Solution. *Polym. Chem.* **2022**, *13* (12), 1751−1762.

(31) Kumar, A. A.; Som, A.; Longo, P.; Sudhakar, C.; Bhuin, R. G.; Gupta, S. S.; Anshup; Sankar, M. U.; Chaudhary, A.; Kumar, R.; Pradeep, T. Confined Metastable 2-Line Ferrihydrite for Affordable Point-of-Use Arsenic-Free Drinking Water. *Adv. Mater.* **2017**, *29* (7), No. 1604260.

(32) Zhuang, S.; Zhu, K.; Wang, J. Fibrous Chitosan/Cellulose Composite as an Efficient Adsorbent for Co(II) Removal. *J. Clean. Prod.* **2021**, *285*, No. 124911.

(33) Dai, Z.; Sun, Y.; Zhang, H.; Ding, D.; Li, L. Rational Synthesis of Polyamidoxime/Polydopamine-Decorated Graphene Oxide Composites for Efficient Uranium(VI) Removal from Mine Radioactive Wastewater. *Ind. Eng. Chem. Res.* **2019**, *58* (41), 19280−19291.

(34) Wang, J.; Zhuang, S. Removal of Various Pollutants from Water and Wastewater by Modified Chitosan Adsorbents. *Crit. Rev. Environ. Sci. Technol.* **2017**, *47* (23), 2331−2386.

(35) Khalil, T. E.; Abdel-Salam, A. H.; Mohamed, L. A.; El-Meligy, E.; El-Dissouky, A. Crosslinked Modified Chitosan Biopolymer for Enhanced Removal of Toxic Cr(VI) from Aqueous Solution. *Int. J. Biol. Macromol.* **2023**, *234*, No. 123719.

(36) Allouss, D.; Essamlali, Y.; Chakir, A.; Khadhar, S.; Zahouily, M. Effective Removal of Cu(II) from Aqueous Solution over Graphene Oxide Encapsulated Carboxymethylcellulose-Alginate Hydrogel Microspheres: Towards Real Wastewater Treatment Plants. *Environ. Sci. Pollut. Res.* **2020**, *27* (7), 7476−7492.

(37) Pettignano, A.; Charlot, A.; Fleury, E. Solvent-Free Synthesis of Amidated Carboxymethyl Cellulose Derivatives: Effect on the Thermal Properties. *Polymers* **2019**, *11* (7), 1227.

(38) Manzoor, K.; Ahmad, M.; Ahmad, S.; Ikram, S. Synthesis, Characterization, Kinetics, and Thermodynamics of EDTA-Modified Chitosan-Carboxymethyl Cellulose as Cu(II) Ion Adsorbent. *ACS Omega* **2019**, *4* (17), 17425−17437.

(39) Hamilton, G. S. *P*-Toluenesulfonic Acid. In *Encyclopedia of Reagents for Organic Synthesis*; John Wiley & Sons, Ltd: Chichester, UK, 2001; p rt134. DOI: 10.1002/047084289X.rt134.

(40) Mollick, S.; Saurabh, S.; More, Y. D.; Fajal, S.; Shirolkar, M. M.; Mandal, W.; Ghosh, S. K. Benchmark Uranium Extraction from Seawater Using an Ionic Macroporous Metal−Organic Framework. *Energy Environ. Sci.* **2022**, *15* (8), 3462−3469.

(41) Wang, C.; Huang, D.; He, F.; Jin, T.; Huang, B.; Xu, J.; Qian, Y. Efficient Removal of Uranium(VI) from Aqueous Solutions by Triethylenetetramine-Functionalized Single-Walled Carbon Nanohorns. *ACS Omega* **2020**, *5* (43), 27789−27799.

(42) Priya, S.; Ilaiyaraja, P.; Priyadarshini, N.; Subalekha, N. Effective Removal of Uranium (VI) Using Magnetic Acid Functionalized Fe3O4@TiO2 Nanocomposite from Aqueous Solutions. *Process Saf. Environ. Prot.* **2023**, *178*, 480−493.

(43) Sun, Q.; Aguila, B.; Perman, J.; Ivanov, A. S.; Bryantsev, V. S.; Earl, L. D.; Abney, C. W.; Wojtas, L.; Ma, S. Bio-Inspired Nano-Traps for Uranium Extraction from Seawater and Recovery from Nuclear Waste. *Nat. Commun.* **2018**, *9* (1), 1644.

(44) Galindo, C.; Nero, M. D.; Barillon, R.; Halter, E.; Made, B. Mechanisms of Uranyl and Phosphate (Co)Sorption: Complexation and Precipitation at α-Al2O3 Surfaces. *J. Colloid Interface Sci.* **2010**, *347* (2), 282−289.

(45) Kushwaha, S.; Sreedhar, B.; Padmaja, P. XPS, EXAFS, and FTIR As Tools To Probe the Unexpected Adsorption-Coupled Reduction of U(VI) to U(V) and U(IV) on *Borassus Flabellifer* -Based Adsorbents. *Langmuir* **2012**, *28* (46), 16038−16048.

(46) Wang, Y.; Ai, Y.; Liu, X.; Chen, B.; Zhang, Y. Indole-Functionalized Cross-Linked Chitosan for Effective Uptake of Uranium(vi) from Aqueous Solution. *Polym. Chem.* **2022**, *13* (12), 1751−1762.

(47) Sabatini, M. T.; Boulton, L. T.; Sneddon, H. F.; Sheppard, T. D. A Green Chemistry Perspective on Catalytic Amide Bond Formation. *Nat. Catal.* **2019**, *2* (1), 10−17.

(48) Nakajima, N.; Ikada, Y. Mechanism of Amide Formation by Carbodiimide for Bioconjugation in Aqueous Media. *Bioconjugate Chem.* **1995**, *6* (1), 123−130.

(49) Noorian, S. A.; Hemmatinejad, N.; Navarro, J. A. R. Ligand Modified Cellulose Fabrics as Support of Zinc Oxide Nanoparticles for UV Protection and Antimicrobial Activities. *Int. J. Biol. Macromol.* **2020**, *154*, 1215−1226.

(50) Zhang, X.; Zhang, L.; Wang, Q.; Xin, Q.; Xiong, Y.; Wang, H. Selective, Rapid Extraction of Uranium from Aqueous Solution by Porous Chitosan−Phosphorylated Chitosan−Amidoxime Macroporous Resin Composite and Differential Charge Calculation. *Int. J. Biol. Macromol.* **2023**, *253*, No. 126661.

(51) Samsonowicz, M.; Hrynaszkiewicz, T.; Świsłocka, R.; Regulska, E.; Lewandowski, W. Experimental and Theoretical IR, Raman, NMR Spectra of 2-, 3- and 4-Aminobenzoic Acids. *J. Mol. Struct.* **2005**, *744*−*747*, 345−352.

(52) Verma, S.; Dutta, R. K. Development of Cysteine Amide Reduced Graphene Oxide (CARGO) Nano-Adsorbents for Enhanced Uranyl Ions Removal from Aqueous Medium. *J. Environ. Chem. Eng.* **2017**, *5* (5), 4547−4558.

(53) Cai, Y.; Chen, L.; Yang, S.; Xu, L.; Qin, H.; Liu, Z.; Chen, L.; Wang, X.; Wang, S. Rational Synthesis of Novel Phosphorylated Chitosan-Carboxymethyl Cellulose Composite for Highly Effective Decontamination of U(VI). *ACS Sustain. Chem. Eng.* **2019**, *7* (5), 5393−5403.

(54) D'Orsi, R.; Canale, V. C.; Cancelliere, R.; Hassan Omar, O.; Mazzuca, C.; Micheli, L.; Operamolla, A. Tailoring the Chemical Structure of Cellulose Nanocrystals by Amine Functionalization. *Eur. J. Org. Chem.* **2023**, *26* (11), No. e202201457.

(55) Kushwaha, S.; Mane, M.; Ravindranathan, S.; Das, A. Polymer Nanorings with Uranium Specific Clefts for Selective Recovery of Uranium from Acidic Effluents via Reductive Adsorption. *ACS Sens.* **2020**, *5* (10), 3254−3263.

(56) Malla, B. K.; Vishwakarma, G.; Chowdhury, S.; Nayak, S. K.; Yamijala, S. S. R. K. C.; Pradeep, T. Formation and Dissociation of Dimethyl Ether Clathrate Hydrate in Interstellar Ice Mimics. *J. Phys. Chem. C* **2024**, *128* (6), 2463−2470.

(57) Lu, G.; Forbes, T. Z.; Haes, A. J. Evaluating Best Practices in Raman Spectral Analysis for Uranium Speciation and Relative

Abundance in Aqueous Solutions. *Anal. Chem.* **2016**, *88* (1), 773−780.
(58) Sánchez, C.; Bustos, C.; Alvarado, F.; Schott, E.; Gatica, N.; Bernede, J.-C. Synthesis, Characterization and Properties of Polymers Containing Simultaneously the Imine and Amide Moieties. *E-Polym.* **2007**, 7 (1). DOI: 10.1515/epoly.2007.7.1.434.
(59) Du, W.-Q.; Fu, T.; Li, X.-L.; Li, Y.; Deng, C.; Wang, X.-L.; Wang, Y.-Z. High-Performance Biobased Polyesters with High Gas Barrier, Glass Transition Temperature, and Tensile Strength Enabled by Hydrogen Bonds and Flexible Segments. *ACS Sustain. Chem. Eng.* **2022**, *10* (43), 14240−14247.
(60) Dutta, R. K.; Shaida, Md. A.; Singla, K.; Das, D. Highly Efficient Adsorptive Removal of Uranyl Ions by a Novel Graphene Oxide Reduced by Adenosine 5′-Monophosphate (RGO-AMP). *J. Mater. Chem. A* **2019**, 7 (2), 664−678.
(61) Cai, Y.; Wu, C.; Liu, Z.; Zhang, L.; Chen, L.; Wang, J.; Wang, X.; Yang, S.; Wang, S. Fabrication of a Phosphorylated Graphene Oxide−Chitosan Composite for Highly Effective and Selective Capture of U(vi). *Environ. Sci. Nano* **2017**, *4* (9), 1876−1886.
(62) Badry, R.; El-Nahass, M. M.; Nada, N.; Elhaes, H.; Ibrahim, M. A. Structural and UV-Blocking Properties of Carboxymethyl Cellulose Sodium/CuO Nanocomposite Films. *Sci. Rep.* **2023**, *13* (1), 1123.
(63) Sun, L.; Hu, K.; Jin, S.; Lu, Y.; Xu, C.; Liu, B.; Wang, D.; Xia, G. Single-Crystal and Molecular Structures of Five Hydrogen-Bonding Supramolecular Salts Based on 4-Aminobenzoic Acid, 2-Aminobenzoic Acid and Acidic Components. *J. Mol. Struct.* **2019**, *1178*, 229−241.
(64) Abomosallam, M.; Elalfy, M.; Zheng, Z.; Nagata, K.; Suzuki, M. Adsorption Kinetics and Thermodynamics of Toxic Metal Ions onto Chitosan Nanoparticles Extracted from Shrimp Shells. *Nanotechnol. Environ. Eng.* **2022**, *7* (1), 35−47.
(65) Husnain, S. M.; Kim, H. J.; Um, W.; Chang, Y.-Y.; Chang, Y.-S. Superparamagnetic Adsorbent Based on Phosphonate Grafted Mesoporous Carbon for Uranium Removal. *Ind. Eng. Chem. Res.* **2017**, *56* (35), 9821−9830.
(66) Gómez, N.; Silva, G.; Wilhelm, H.; Wypych, F. Zn2Al Layered Double Hydroxides Intercalated with Nitrate and P-Aminobenzoate as Ultraviolet Protective Agents in Low-Density Polyethylene Nanocomposites and Natural Insulating Oils. *J. Braz. Chem. Soc.* **2020**, DOI: 10.21577/0103-5053.20190262.
(67) Jin, H.-X.; Xu, H.; Wang, N.; Yang, L.-Y.; Wang, Y.-G.; Yu, D.; Ouyang, X.-K. Fabrication of Carboxymethylcellulose/Metal-Organic Framework Beads for Removal of Pb(II) from Aqueous Solution. *Materials* **2019**, *12* (6), 942.
(68) Poornachandhra, C.; Jayabalakrishnan, R. M.; Prasanthrajan, M.; Balasubramanian, G.; Lakshmanan, A.; Selvakumar, S.; John, J. E. Cellulose-Based Hydrogel for Adsorptive Removal of Cationic Dyes from Aqueous Solution: Isotherms and Kinetics. *RSC Adv.* **2023**, *13* (7), 4757−4774.
(69) Wang, Y.; Lin, Z.; Zhu, J.; Liu, J.; Yu, J.; Liu, Q.; Chen, R.; Li, Y.; Wang, J. Enhancing Adsorption Performance and Selectivity for Uranium by Constructing Biaxial Adsorption Sites on Eco-Friendly Bamboo Strips. *Sep. Purif. Technol.* **2023**, *315*, No. 123727.
(70) Meng, F.; Yuan, G.; Larson, S. L.; Ballard, J. H.; White, J. R.; Arslan, Z.; Han, F. X. Kinetics and Thermodynamics of Uranium (VI) Adsorption onto Humic Acid Derived from Leonardite. *Int. J. Environ. Res. Public. Health* **2019**, *16* (9), 1552.
(71) Ivanov, A. S.; Leggett, C. J.; Parker, B. F.; Zhang, Z.; Arnold, J.; Dai, S.; Abney, C. W.; Bryantsev, V. S.; Rao, L. Origin of the Unusually Strong and Selective Binding of Vanadium by Polyamidoximes in Seawater. *Nat. Commun.* **2017**, *8* (1), 1560.
(72) Zhang, Y.; Wang, Y.; Dong, Z.; Wang, Y.; Liu, Y.; Cao, X.; Zhang, Z.; Xu, C.; Wang, N.; Liu, Y. Boosting Uranium Extraction from Seawater by Micro-Redox Reactors Anchored in a Seaweed-like Adsorbent. *Nat. Commun.* **2024**, *15* (1), 9124.
(73) Emre, D.; Zorer, Ö. S.; Bilici, A.; Budak, E.; Yilmaz, S.; Kilic, N. C.; Sogut, E. G. Adsorption of Uranium (VI) from Aqueous Solutions Using Boron Nitride/Polyindole Composite Adsorbent. *J. Appl. Polym. Sci.* **2024**, *141* (4), No. e54856.
(74) Zhao, M.; Tesfay Reda, A.; Zhang, D. Reduced Graphene Oxide/ZIF-67 Aerogel Composite Material for Uranium Adsorption in Aqueous Solutions. *ACS Omega* **2020**, *5* (14), 8012−8022.
(75) Szlachta, M.; Neitola, R.; Peräniemi, S.; Vepsäläinen, J. Effective Separation of Uranium from Mine Process Effluents Using Chitosan as a Recyclable Natural Adsorbent. *Sep. Purif. Technol.* **2020**, *253*, No. 117493.
(76) Sun, Z.; Chen, D.; Chen, B.; Kong, L.; Su, M. Enhanced Uranium(VI) Adsorption by Chitosan Modified Phosphate Rock. *Colloids Surf. Physicochem. Eng. Asp.* **2018**, *547*, 141−147.
(77) Anirudhan, T. S.; Lekshmi, G. S.; Shainy, F. Synthesis and Characterization of Amidoxime Modified Chitosan/Bentonite Composite for the Adsorptive Removal and Recovery of Uranium from Seawater. *J. Colloid Interface Sci.* **2019**, *534*, 248−261.
(78) Bai, J.; Ma, X.; Yan, H.; Zhu, J.; Wang, K.; Wang, J. A Novel Functional Porous Organic Polymer for the Removal of Uranium from Wastewater. *Microporous Mesoporous Mater.* **2020**, *306*, No. 110441.
(79) Tellería-Narvaez, A.; Talavera-Ramos, W.; Santos, L. D.; Arias, J.; Kinbaum, A.; Luca, V. Functionalized Natural Cellulose Fibres for the Recovery of Uranium from Seawater. *RSC Adv.* **2020**, *10* (11), 6654−6657.
(80) Busca, G. Bases and Basic Materials in Industrial and Environmental Chemistry: A Review of Commercial Processes. *Ind. Eng. Chem. Res.* **2009**, *48* (14), 6486−6511.
(81) Elschner, T.; Lüdecke, C.; Kalden, D.; Roth, M.; Löffler, B.; Jandt, K. D.; Heinze, T. Zwitterionic Cellulose Carbamate with Regioselective Substitution Pattern: A Coating Material Possessing Antimicrobial Activity. *Macromol. Biosci.* **2016**, *16* (4), 522−534.
(82) Wang, L.; Liu, X.; Tan, W.; Li, Q.; Guo, Z.; Zhang, J. Preparation and Antioxidant Activity of Novel Chitosan Oligosaccharide Quinolinyl Urea Derivatives. *Carbohydr. Res.* **2022**, *521*, No. 108678.